A Three Dimensional Numerical Model of the Flow over a Complex Terrain with Height Variation less than 100m

Mingyuan Du,
(National Institute of Agro-Environmental Sciences of Japan)
Peiming Wu,
(National Space Development Agency of Japan)
Taichi Maki and Shigeto Kawashima
(National Institute of Agro-Environmental Sciences of Japan)

Abstract In order to clarify the effects of windbreaks on the flow and to determine where to set windbreaks for best prevention of wind erosion in a complex terrain, a three-dimensional numerical model for simulating wind distribution over a real complex terrain with a variation of relative height less than 100m is developed. The three-dimensional, time-dependent Navier-Stokes equation written with generalized coordinates and the Smagorinsky-type scheme for turbulent parameterization are use in the model. Numerical simulations of windbreak effect on wind speed distribution over a sand dune are carried out by erecting windbreak hedges at different places. The influence of topography and windbreaks on wind distribution, for example the location of the maximum wind speed reduction, are well simulated. Thus, the best setting place of windbreak for prevention of wind erosion may be decided by simulating the wind distribution around real terrain using the model. An example, using a 2m high windbreak hedge for preventing sand shifting around a barchan sand dune which is 5m high, 64m wide and 96m long, is given and effect of the windbreak hedge is discussed. The simulation results show that the best place should be at 18m-22m in front of the top of the sand dune.

1. INTRODUCTION

Windbreaks including forests, nets, fences and hedges have been used for centuries for prevention of wind erosion, increasing productivity, promoting environmental sustainability, and improving the quality of life throughout the world. All the effectiveness of a windbreak may be illustrated by the modification of air flow patterns and so that improvement of micro-climate. Reviews of recent researches have been given by van Eimern at al. (1964), McNaughton (1988), Heisler and DeWalle (1988). Recently, we have done some works on windbreak effects in arid land (Du and Maki, 1993, 1997; Maki et al., 1993, 1995, 1997) and realized that it is necessary to clarify the effects of windbreaks on the flow over complex terrain. As shown by some recent useful numerical simulations (e.g. Wilson, 1985; Wang and Takle, 1995a, 1995b, 1996) and wind tunnel investigations (e.g. Maki, 1982; Judd et al., 1996), it is relatively easy to observe or to estimate the effect of windbreak when the windbreak located in a flat or smoothed place. However, It is difficult to know the effect of a windbreak on wind and to determine where to set windbreak for best prevention of wind erosion in a complex terrain or even around a sand dune. To our knowledge, there are no theoretical and numerical studies that address boundary layer flow near windbreaks over complex terrain, although some works have shown numerical simulation of wind flow over a sand dune and sand dune movement (e.g. Wippermann and Gross, 1986; Fisher and Galdies, 1988).

Our purpose is establish a simple numerical model to simulate the mean air flow near windbreaks over complex terrain in order to clarify the effects of windbreaks on the flow and to determine where to set windbreaks for best prevention of wind erosion. This paper presents a three-dimensional numerical model for simulating mean wind distribution over a real complex terrain with a variation of relative height less than 100m and some numerical simulation results of windbreak hedge effect on wind speed distribution around a barchan sand dune with 5m high and 96m long by erecting windbreaks at different place. The influences of topography and windbreaks on wind are well simulated.

2. MODEL DESCRIPTION

2.1 The Equations

For our purpose, we consider that windbreak is about 10m and that the variation of complex terrain is less than 100m, which are less than the height of the atmosphere boundary layer, so the effect of Coriolis force and thermodynamic variety deduce by topography and windbreak may be neglected. We limit our attention to neutral stratification and, in order to catch the influence of sharp variation of topography, use generalized terrain-following coordinates (ξ, ψ, ζ) which is defined as follows. The vertical line ζ is orthogonalized to ground surface and $\zeta=0$ is at ground surface, orthogonal relations are also exited between vertical coordinate line and other coordinate lines, ξ, ψ. Thus, we have following relations between the generalized terrain-following coordinates (ξ, ψ, ζ) and Cartesian coordinate (x, y, z).

$$\begin{aligned} U &= \xi_x \cdot u + \xi_y \cdot v + \xi_z \cdot w \\ V &= \psi_x \cdot u + \psi_y \cdot v + \psi_z \cdot w \\ W &= \zeta_x \cdot u + \xi_y \cdot v + \xi_z \cdot w \end{aligned} \tag{1}$$

$$J = \begin{vmatrix} \xi_x & \xi_y & \xi_z \\ \psi_x & \psi_y & \psi_z \\ \zeta_x & \zeta_y & \zeta_z \end{vmatrix} \tag{2}$$

where U, V, W are the generalized terrain-following coordinates (ξ, ψ, ζ) component velocities respectively,

u, v, w are Cartesian coordinates (x, y, z) component velocities respectively, ξ_x, ξ_y, ξ_z, ψ_x, ψ_y, ψ_z and ζ_x, ζ_y, ζ_z, are differential calculus for the subscript (x, y, z, e.g. $\xi_x = \partial\xi / \partial x$ etc.), J is Jacobian.

Using Equations (1) and (2), and the above limitation, under the Boussinesq approximation, the three-dimensional, non-hydrostatic, incompressible atmospheric continuity equation and equations of motion in the generalized terrain-following coordinates (ξ, ψ, ζ) may be written as

$$\frac{\partial(U/J)}{\partial\xi}+\frac{\partial(V/J)}{\partial\psi}+\frac{\partial(W/J)}{\partial\zeta}=0 \tag{3}$$

$$\begin{aligned}&\frac{\partial(u_i/J)}{\partial t}+\frac{\partial(Uu_i/J)}{\partial\xi}+\frac{\partial(Vu_i/J)}{\partial\psi}+\frac{\partial(Wu_i/J)}{\partial\zeta}\\&=-\frac{\partial(\xi_i P/J)}{\partial\xi}-\frac{\partial(\psi_i P/J)}{\partial\psi}-\frac{\partial(\zeta_i P/J)}{\partial\zeta}\\&+\frac{\partial((\xi_x\tau_{i1}+\xi_y\tau_{i2}+\xi_z\tau_{i3})/J)}{\partial\xi}+\frac{\partial((\psi_x\tau_{i1}+\psi_y\tau_{i2}+\psi_z\tau_{i3})/J)}{\partial\psi}\\&+\frac{\partial((\zeta_x\tau_{i1}+\zeta_y\tau_{i2}+\zeta_z\tau_{i3})/J)}{\partial\zeta}\\&(i=1,2,3;\ u_i=u_1,u_2,u_3=u,v,w)\end{aligned} \tag{4}$$

where $P=p/\rho_0$ is air pressure, τ_{ij} (i, j=1, 2, 3) is the trace-free subgrid-scale Reynolds stress.

2.2 Subgrid-scale Parameterization

The Smagorinsky-type subgrid scheme (1963) are use in our model considering the balance between shear production and dissipation by topography and windbreak. Thus, we have subgrid-scale Reynolds stress in the generalized terrain-following coordinates (ξ, ψ, ζ) as follows.

$$\begin{aligned}&\tau_{ij}=\upsilon\cdot D_{ij}\\&D_{ij}=(\xi_i\cdot\frac{\partial u_i}{\partial\xi}+\psi_i\cdot\frac{\partial u_i}{\partial\psi}+\zeta_i\cdot\frac{\partial u_i}{\partial\zeta}\\&+\xi_j\cdot\frac{\partial u_j}{\partial\xi}+\psi_j\cdot\frac{\partial u_j}{\partial\psi}+\zeta_j\cdot\frac{\partial u_j}{\partial\zeta}\\&\upsilon=(C_s\Delta)^2(0.5\sum_{i,j=1}^{3}D_{ij}^{\ 2})^{1/2}\\&\Delta^3=(\Delta x\Delta y\Delta z)=(\Delta\xi\Delta\eta\Delta\zeta)/J\\&C_s=0.12\end{aligned} \tag{5}$$

where C_s is called as Smagorinsky constant. At the surface boundary, we assume that neutral stratification can be applied to ζ axis, and

$$\begin{aligned}&u_*=\frac{k(u_1^{\ 2}+v_1^{\ 2})^{1/2}}{\ln(\Delta z/z_0)}\\&K_m=k\Delta z u_*\end{aligned} \tag{6}$$

where u_* is friction velocity, k is Karman constant (0.4), u_1 and v_1 are wind speed conponent at first level Z_1, z_0 is roughness length. Thus,

$$\begin{aligned}&\tau_{ij}=\upsilon\cdot D_{ij}\\&D_{ij}=\zeta_i\cdot\frac{\partial u_i}{\partial\zeta}+\zeta_j\cdot\frac{\partial u_j}{\partial\zeta}\\&\upsilon=k^2\Delta(\sum_{i=1}^{3}u_i^{\ 2})^{1/2}/\ln^2(\frac{\Delta}{z_0})\\&\Delta=(x_1^{\ 2}+y_1^{\ 2}+z_1^{\ 2})^{1/2}\Delta\zeta\end{aligned} \tag{7}$$

where (x_1, y_1, z_1) is component of Z_1, u_1 is wind speed at Z_1.

2.3 Numerical Method

2.3.1 Grids Formation

The initial horizontal grid is formed by introducing mesh topography data and the interval of the grids is determined depending on topography data and calculation problem. The vertical grid is formed by making the transformed coordinates from given terrain using elliptic equations. Three Poisson like equations are

$$\begin{aligned}&a\frac{\partial^2X}{\partial\xi^2}+b\frac{\partial^2X}{\partial\psi^2}+c\frac{\partial^2X}{\partial\zeta^2}+2d\frac{\partial^2X}{\partial\xi\partial\psi}+2e\frac{\partial^2X}{\partial\xi\partial\zeta}+2f\frac{\partial^2X}{\partial\psi\partial\zeta}=-J^2\frac{\partial X}{\partial\zeta}R(\zeta)\\&a\frac{\partial^2Y}{\partial\xi^2}+b\frac{\partial^2Y}{\partial\psi^2}+c\frac{\partial^2Y}{\partial\zeta^2}+2d\frac{\partial^2Y}{\partial\xi\partial\psi}+2e\frac{\partial^2Y}{\partial\xi\partial\zeta}+2f\frac{\partial^2Y}{\partial\psi\partial\zeta}=-J^2\frac{\partial Y}{\partial\zeta}R(\zeta)\\&a\frac{\partial^2Z}{\partial\xi^2}+b\frac{\partial^2Z}{\partial\psi^2}+c\frac{\partial^2Z}{\partial\zeta^2}+2d\frac{\partial^2Z}{\partial\xi\partial\psi}+2e\frac{\partial^2Z}{\partial\xi\partial\zeta}+2f\frac{\partial^2Z}{\partial\psi\partial\zeta}=-J^2\frac{\partial Z}{\partial\zeta}R(\zeta)\end{aligned} \tag{8}$$

and

$$\begin{aligned}&a=(\frac{\partial Y}{\partial\psi}\frac{\partial Z}{\partial\zeta}-\frac{\partial Y}{\partial\zeta}\frac{\partial Z}{\partial\psi})^2+(\frac{\partial Z}{\partial\psi}\frac{\partial X}{\partial\zeta}-\frac{\partial Z}{\partial\zeta}\frac{\partial X}{\partial\psi})^2+(\frac{\partial X}{\partial\psi}\frac{\partial Y}{\partial\zeta}-\frac{\partial X}{\partial\zeta}\frac{\partial Z}{\partial\psi})^2\\&b=(\frac{\partial Y}{\partial\xi}\frac{\partial Z}{\partial\zeta}-\frac{\partial Y}{\partial\zeta}\frac{\partial Z}{\partial\xi})^2+(\frac{\partial Z}{\partial\xi}\frac{\partial X}{\partial\zeta}-\frac{\partial Z}{\partial\zeta}\frac{\partial X}{\partial\xi})^2+(\frac{\partial X}{\partial\xi}\frac{\partial Y}{\partial\zeta}-\frac{\partial X}{\partial\zeta}\frac{\partial Y}{\partial\xi})^2\\&c=(\frac{\partial Y}{\partial\xi}\frac{\partial Z}{\partial\psi}-\frac{\partial Y}{\partial\psi}\frac{\partial Z}{\partial\xi})^2+(\frac{\partial Z}{\partial\xi}\frac{\partial X}{\partial\psi}-\frac{\partial Z}{\partial\psi}\frac{\partial X}{\partial\xi})^2+(\frac{\partial X}{\partial\xi}\frac{\partial Y}{\partial\psi}-\frac{\partial X}{\partial\psi}\frac{\partial Z}{\partial\xi})^2\\&d=(\frac{\partial Y}{\partial\psi}\frac{\partial Z}{\partial\zeta}-\frac{\partial Y}{\partial\zeta}\frac{\partial Z}{\partial\psi})(\frac{\partial Y}{\partial\xi}\frac{\partial Z}{\partial\zeta}-\frac{\partial Y}{\partial\zeta}\frac{\partial Z}{\partial\xi})+(\frac{\partial Z}{\partial\psi}\frac{\partial X}{\partial\zeta}-\frac{\partial Z}{\partial\zeta}\frac{\partial X}{\partial\psi})\\&(\frac{\partial Z}{\partial\xi}\frac{\partial X}{\partial\zeta}-\frac{\partial Z}{\partial\zeta}\frac{\partial X}{\partial\xi})+(\frac{\partial X}{\partial\psi}\frac{\partial Y}{\partial\zeta}-\frac{\partial X}{\partial\zeta}\frac{\partial Y}{\partial\psi})(\frac{\partial X}{\partial\xi}\frac{\partial Y}{\partial\zeta}-\frac{\partial X}{\partial\zeta}\frac{\partial Y}{\partial\xi})\\&e=(\frac{\partial Y}{\partial\xi}\frac{\partial Z}{\partial\psi}-\frac{\partial Y}{\partial\psi}\frac{\partial Z}{\partial\xi})(\frac{\partial Y}{\partial\psi}\frac{\partial Z}{\partial\zeta}-\frac{\partial Y}{\partial\zeta}\frac{\partial Z}{\partial\psi})+(\frac{\partial Z}{\partial\xi}\frac{\partial X}{\partial\psi}-\frac{\partial Z}{\partial\psi}\frac{\partial X}{\partial\xi})\\&(\frac{\partial Z}{\partial\psi}\frac{\partial X}{\partial\zeta}-\frac{\partial Z}{\partial\zeta}\frac{\partial X}{\partial\psi})+(\frac{\partial X}{\partial\xi}\frac{\partial Y}{\partial\psi}-\frac{\partial X}{\partial\psi}\frac{\partial Y}{\partial\xi})(\frac{\partial X}{\partial\psi}\frac{\partial Y}{\partial\zeta}-\frac{\partial X}{\partial\zeta}\frac{\partial Y}{\partial\psi})\\&f=(\frac{\partial Y}{\partial\xi}\frac{\partial Z}{\partial\zeta}-\frac{\partial Y}{\partial\zeta}\frac{\partial Z}{\partial\xi})(\frac{\partial Y}{\partial\xi}\frac{\partial Z}{\partial\psi}-\frac{\partial Y}{\partial\psi}\frac{\partial Z}{\partial\xi})+(\frac{\partial Z}{\partial\xi}\frac{\partial X}{\partial\zeta}-\frac{\partial Z}{\partial\zeta}\frac{\partial X}{\partial\xi})\\&(\frac{\partial Z}{\partial\xi}\frac{\partial X}{\partial\psi}-\frac{\partial Z}{\partial\psi}\frac{\partial X}{\partial\xi})+(\frac{\partial X}{\partial\xi}\frac{\partial Y}{\partial\zeta}-\frac{\partial X}{\partial\zeta}\frac{\partial Y}{\partial\xi})(\frac{\partial X}{\partial\xi}\frac{\partial Y}{\partial\psi}-\frac{\partial X}{\partial\psi}\frac{\partial Y}{\partial\xi})\\&J=\frac{\partial X}{\partial\xi}\frac{\partial Y}{\partial\psi}\frac{\partial Z}{\partial\zeta}+\frac{\partial X}{\partial\psi}\frac{\partial Y}{\partial\zeta}\frac{\partial Z}{\partial\xi}+\frac{\partial X}{\partial\zeta}\frac{\partial Y}{\partial\xi}\frac{\partial Z}{\partial\psi}-\frac{\partial X}{\partial\zeta}\frac{\partial Y}{\partial\psi}\frac{\partial Z}{\partial\xi}-\\&\frac{\partial X}{\partial\psi}\frac{\partial Y}{\partial\xi}\frac{\partial Z}{\partial\zeta}-\frac{\partial X}{\partial\xi}\frac{\partial Y}{\partial\zeta}\frac{\partial Z}{\partial\psi}\\&R(\zeta)=-\alpha e^{-\beta\zeta}\end{aligned} \tag{9}$$

where (X, Y, Z) are the Cartesian coordinates in the transformed generalized terrain-following coordinate grid. R(ζ) is a grid control function for attraction of coordinate line to surface. α, β are empirical parameters. The number of vertical level and general interval can be got by input parameters. In the simulation α, β are taken as 0.1 and 0.2,

respectively. By using the function and iterating of the Poisson like equations, grids (X, Y, Z) can be obtained. The boundary condition of the Poisson equations are at the grid boundary (ξ=0, ψ=0, ξ=ξ_{max}, ψ=ψ_{max}) and also at the top boundary (ζ=z=ζ_{max}) the two coordinates become the same. That is

$$\begin{aligned} \partial Y/\partial\xi = \partial Z/\partial\xi = 0 \quad & \text{for} \quad \xi=0,\ \xi=\xi_{max}, \\ \partial X/\partial\psi = \partial Z/\partial\psi = 0 \quad & \text{for} \quad \psi=0,\ \psi=\psi_{max}, \\ \partial X/\partial\zeta = \partial Y/\partial\zeta = 0 \quad & \text{for} \quad \zeta=0,\ \zeta=\zeta_{max}, \end{aligned} \tag{10}$$

For ground boundary, ζ=0 is at ground surface, and due to orthogonal relations between vertical coordinate line and other coordinate lines at the surface, we have

$$\begin{aligned} & Z = z_s(X(\xi,\psi,0), Y(\xi,\psi,0)) \\ & \frac{\partial X}{\partial\xi}\frac{\partial X}{\partial\zeta} + \frac{\partial Y}{\partial\xi}\frac{\partial Y}{\partial\zeta} = -\frac{\partial Z}{\partial\xi}\frac{\partial Z}{\partial\zeta} \\ & \frac{\partial X}{\partial\psi}\frac{\partial X}{\partial\zeta} + \frac{\partial Y}{\partial\psi}\frac{\partial Y}{\partial\zeta} = -\frac{\partial Z}{\partial\psi}\frac{\partial Z}{\partial\zeta} \end{aligned} \tag{11}$$

After we get the grid coordinates, ξ_x, ξ_y, ξ_z, ψ_x, ψ_y, ψ_z and ζ_x, ζ_y, ζ_z, and Jacobian can be get:

$$\begin{aligned} \xi_x &= \frac{\partial\xi}{\partial x} = \left(\frac{\partial Y}{\partial\psi}\frac{\partial Z}{\partial\zeta} - \frac{\partial Y}{\partial\zeta}\frac{\partial Z}{\partial\psi}\right)/J \\ \xi_y &= \frac{\partial\xi}{\partial y} = \left(\frac{\partial Z}{\partial\psi}\frac{\partial X}{\partial\zeta} - \frac{\partial Z}{\partial\zeta}\frac{\partial X}{\partial\psi}\right)/J \\ \xi_z &= \frac{\partial\xi}{\partial z} = \left(\frac{\partial X}{\partial\psi}\frac{\partial Y}{\partial\zeta} - \frac{\partial X}{\partial\zeta}\frac{\partial Y}{\partial\psi}\right)/J \\ \psi_x &= \frac{\partial\psi}{\partial x} = \left(\frac{\partial Y}{\partial\zeta}\frac{\partial Z}{\partial\xi} - \frac{\partial Y}{\partial\xi}\frac{\partial Z}{\partial\zeta}\right)/J \\ \psi_y &= \frac{\partial\psi}{\partial y} = \left(\frac{\partial Z}{\partial\zeta}\frac{\partial X}{\partial\xi} - \frac{\partial Z}{\partial\xi}\frac{\partial X}{\partial\zeta}\right)/J \\ \psi_z &= \frac{\partial\psi}{\partial z} = \left(\frac{\partial X}{\partial\zeta}\frac{\partial Y}{\partial\xi} - \frac{\partial X}{\partial\xi}\frac{\partial Y}{\partial\zeta}\right)/J \\ \zeta_x &= \frac{\partial\zeta}{\partial x} = \left(\frac{\partial Y}{\partial\xi}\frac{\partial Z}{\partial\psi} - \frac{\partial Y}{\partial\psi}\frac{\partial Z}{\partial\xi}\right)/J \\ \zeta_y &= \frac{\partial\zeta}{\partial y} = \left(\frac{\partial Z}{\partial\xi}\frac{\partial X}{\partial\psi} - \frac{\partial Z}{\partial\psi}\frac{\partial X}{\partial\xi}\right)/J \\ \zeta_z &= \frac{\partial\zeta}{\partial z} = \left(\frac{\partial X}{\partial\xi}\frac{\partial Y}{\partial\psi} - \frac{\partial X}{\partial\psi}\frac{\partial Y}{\partial\xi}\right)/J \\ J &= \frac{\partial X}{\partial\xi}\frac{\partial Y}{\partial\psi}\frac{\partial Z}{\partial\zeta} + \frac{\partial X}{\partial\psi}\frac{\partial Y}{\partial\zeta}\frac{\partial Z}{\partial\xi} + \frac{\partial X}{\partial\zeta}\frac{\partial Y}{\partial\xi}\frac{\partial Z}{\partial\psi} - \frac{\partial X}{\partial\zeta}\frac{\partial Y}{\partial\psi}\frac{\partial Z}{\partial\xi} - \\ & \frac{\partial X}{\partial\psi}\frac{\partial Y}{\partial\xi}\frac{\partial Z}{\partial\zeta} - \frac{\partial X}{\partial\xi}\frac{\partial Y}{\partial\zeta}\frac{\partial Z}{\partial\psi} \end{aligned} \tag{12}$$

2.3.2 Numerical aspect

Main routine controls time integration. Advection terms are calculated with 3rd-oder upstream scheme and other terms with central difference scheme. Pressure is evaluated from solving Poisson equation as follows:

$$\begin{aligned} & \frac{\partial}{\partial\xi}(\xi_x\cdot PX + \xi_y\cdot PY + \xi_z\cdot PZ) + \frac{\partial}{\partial\psi}((\psi_x\cdot PX + \psi_y\cdot PY \\ & + \psi_z\cdot PZ) + \frac{\partial}{\partial\zeta}(\zeta_x\cdot PX + \zeta_y\cdot PY + \zeta_z\cdot PZ) = -r \\ & r = \frac{\partial}{\partial\xi}(\xi_x\cdot AX + \xi_y\cdot AY + \xi_z\cdot AZ) + \frac{\partial}{\partial\psi}((\psi_x\cdot AX + \psi_y\cdot AY \\ & + \psi_z\cdot AZ) + \frac{\partial}{\partial\zeta}(\zeta_x\cdot AX + \zeta_y\cdot AY + \zeta_z\cdot AZ) - \frac{D^t}{\Delta t} \\ & D^t = \frac{\partial}{\partial\xi}(U^t/J) + \frac{\partial}{\partial\psi}(V^t/J) + \frac{\partial}{\partial\zeta}(W^t/J) \end{aligned} \tag{13}$$

where (PX, PY, PZ) are the pressure terms of motion equations and (AX, AY, AZ)) are the advection and diffusion terms of motion equations, D^t is divergent at previous time step t.

2.4 Initial and Boundary Conditions

The initial flow is given automatically by using logarithmic profile to all grids. Simply terrain-following coordinate (x, y, η) is used as initial guess of iteration for coordinate transform. Therefor, topography with vertical surface can not be treated in our model.

The boundary conditions are defined as follows:

(a) At ground surface:
u=v=w=0, $\partial P/\partial\zeta = 0$

(b) At the top of the domain:
$$\frac{\partial u}{\partial\zeta} = \frac{\partial v}{\partial\zeta} = \frac{\partial w}{\partial\zeta} = \frac{\partial P}{\partial\zeta} = 0$$

(c) At the in-flow boundary:
u=u_0, v=v_0, w=w_0, $\partial P/\partial\zeta = 0$

(d) At the out-flow boundary:
$$\frac{\partial u}{\partial\zeta} = \frac{\partial v}{\partial\zeta} = \frac{\partial w}{\partial\zeta} = \frac{\partial P}{\partial\zeta} = 0$$

3. APPLICATIONS TO FLOWS OVER SUND DUNE AND WINDBREAK HEDGES

3.1 Simulation Description

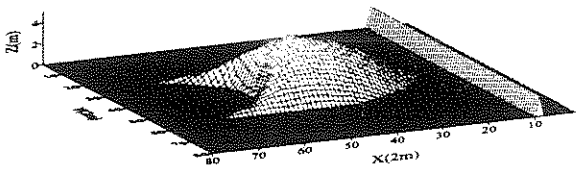

Figure 1: Sand dune, windbreak and grid system used in the simulation.

The mode were used for simulate wind flow around a 5m high windbreak hedge and a barchan sand dune which is 5m high, 64m wide and 96m long. Simulations of windbreak effect on airflow distributions were carried out by erecting 2m high windbreak hedges at different places over and around the sand dune. As shown in Figure 1, the horizontal grids were 80*80 by 2m interval as indicated by letter X and Y. Vertical level was ten (include surface level) and the upper limit of the domain is 18m for quick calculation. The windbreak was 0% porosity 5m or 2m high hedge. As shown in Figure 1, the hedge was 5m or 2m width at the bottom and sharp at the top. The 2m hedge was placed in three different positions for simulation the windbreak effects on airflow over the sand dune: 18m up wind of the dune (x=9), directly in front of the dune (x=18) and 18m upwind of the summit of the dune (x=32), respectively.

The initial wind was 5.0 m/s to the hedge, dune and dune with hedge. That is u_0=5.0m/s, v_0=w_0=0. Time interval was 0.1s. The results of 2,000 step or after 3 minutes and 20 seconds, when the stationary of the flow field was obtained, were used for the evaluation.

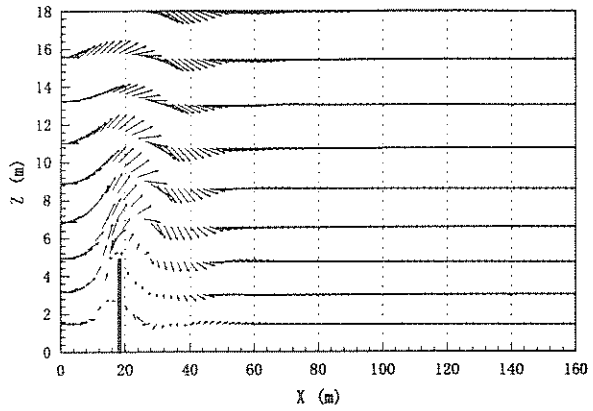

Figure 2: Vertical cross section of wind vectors passes over a 5m high hedge.

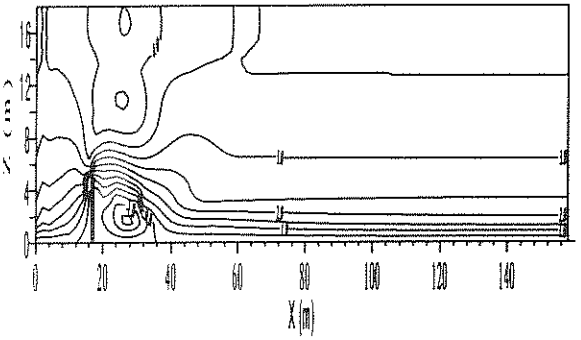

Figure 3: Vertical cross section of wind speed passes over a 5m high hedge.

3.2 Result For 5m High Windbreak Hedge

Figure 2 presents the vertical cross section of wind vectors for airflow pass over the 5m hedge. Figure 3 presents the vertical cross section of wind speed. It is clear that an attached recirculating bubble in the lee appears and wind reduction region and overspeeding region exits. As shown in Figures 2 and 3, a 5m high windbreak hedge reduces wind speed from over 18m (due to no data) upwind to 68m (10H, H is height of windbreak) downwind from its place. This result is in good agreement with observed data. The reversed current has a maximum value at 2H down wind, 0.4H height. The location of separated flow and upstream and downstream regions are in good agreement numerical simulation (Wang and Takle, 1995a), although Wang and Takle presented a result of windbreak of 6% porosity. On the other hand, our results air similar to the wind tunnel experiment results (Maki, 1982). Maki (1982) shown that the location of separated flow was located near 5H and near surface, which was due to a 0.5cm gap exited between the hedge and wind tunnel surface. Thus, our model can be applied to vary sharply changed and nearly vertical surface topography and windbreak.

3.2 Result For 5m High Barchan Sand Dune

Figure 4 shows horizontal distribution of wind speed and Figure 5 shows horizontal distribution of wind vectors of first level (about 1.5m about the ground) around and over a 5m high barchan sand dune. Figure 6 shows horizontal profiles of wind speed at the first 8 level (about 1.5m, 3.2m, 4.9m, 6.8m, 8.9m, 11.0m, 13.2m, and 15.6m) at the center line of the sand dune with topography of the dune (side view, not a cross section). As shown in Figures 4 to 6, there was a speedup region around the windward side of the barchan sand dune and a reduction region in the leeward side of the dune. Wind was strongest on the windward side of the dune summit and grew weaker once it had passed the summit. It was also weak on both wings of the leeward slope of the dune. It can therefore be conjectured that when the wind gains in strength the dune will move or roll downwind retaining its barchan shape.

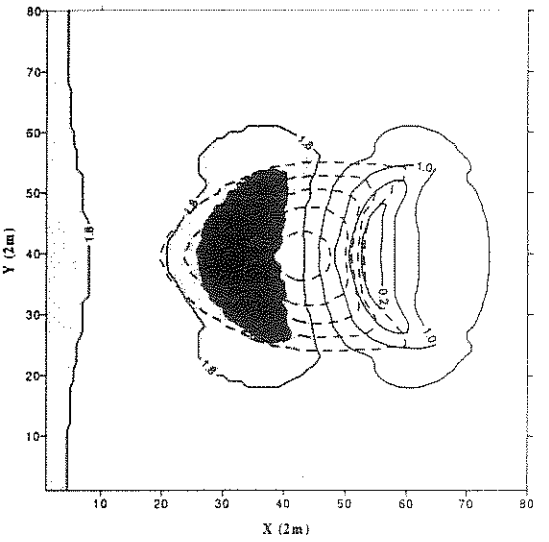

Figure 4: Horizontal distribution of wind speed of first level (about 1.5m above the ground) around and over a 5m high barchan sand dune.

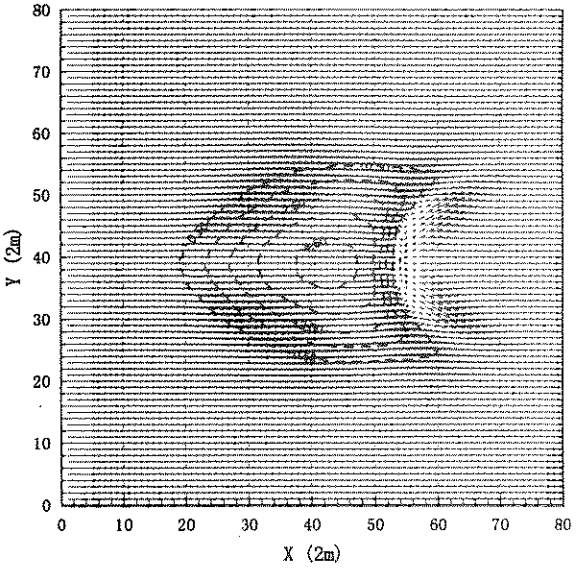

Figure 5: Horizontal distribution of wind vectors of first level (about 1.5m above the ground) around and over a 5m high barchan sand dune.

Comparing to 5m high hedge, the separated region and reversed wind was not clear in the leeward area of the 5m high sand dune. This can be explained by the enfluence of strong overspeeding rigion appeared and the enfluence of the wings of the dune. As shown in Figure 6, the overspeeding area at surface layer began at the foot of the

dune and reaches the summit of the dune. It moved to downward and became smaller with height increasing. Between the two wings in the leeward side, wind was vary weak and was separated to two directions along the wings for keeping the wings move or roll downward. These characteristics of recirculation in the lee of dune are vary different from that simulated by Wippermann and Gross (1986). Wippermann and Gross presented an unreliable reversed flow area, which was as large as the area occupied by the windward side of the dune. Although there is lack of observational data to check our model, it still can conclude that the overspeeding in the winward flow and reduction of leeward flow deduced by barchan sand dune are also well simulated and that the model gives correct prediction of wind distribution over complex terrain.

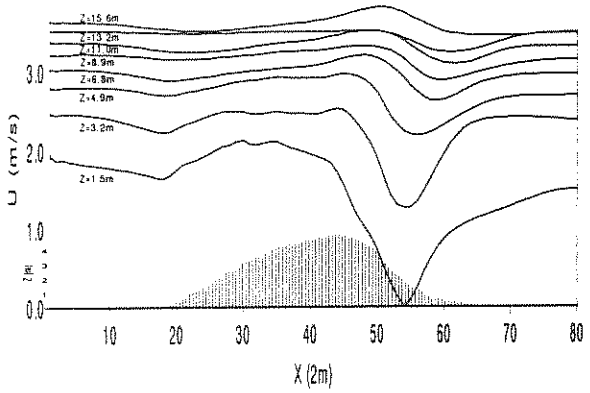

Figure 6: Horizontal profiles of wind speed at the first 8 level at the central line of the sand dune with topography of the dune (side view).

3.4 Effect of 2m High Windbreak Hedge On Airflow Over Sand Dune

Figure 7 shows horizontal distribution of wind speed of first level (about 1.5m about the ground) around and over the barchan sand dune with a 2m high windbreak hedge installed 18m windward of the summit of the dune. Compared with Figure 2, it can be find that the overspeeding area in the windward side, which exited when there is no windbreak, disappeared when the hedge erected 18m windward of the summit of the dune. The area of wind speed over 2.0m/s was only on the windbreak hedge while that was about 1/3 of the area occupied by the windward side of the dune. However, airflow around and over the sand dune did not change much when the 2m high windbreak hedge placed directly in front the dune. When the windbreak hedge was setup 18m windward of the dune, there was no influence on the airflow over sand dune since a 2m high hedge only reduce wind speed from 10m (5H) windward to 20m (10H) leeward of its location. Figure 8 presents the vertical cross section of wind vectors for airflow pass over the dune with the hedge installed 18m windward of the summit of the dune. As shown in Figures 7 and 8, the location of maximum wind speed reduction and the separated flow are well simulated. There were two separated recirculations when a windbreak placed 18m in front of summit of the sand dune. One was small and located in the leeward of windbreak which was deduced by the hedge. Another was big and located in the leeward of the dune which was deduced by the dune. As mentioned above, this separated recirculation was not so large as that simulated by Wippermann and Gross (1986) and was only within 10m in the lee of the dune.

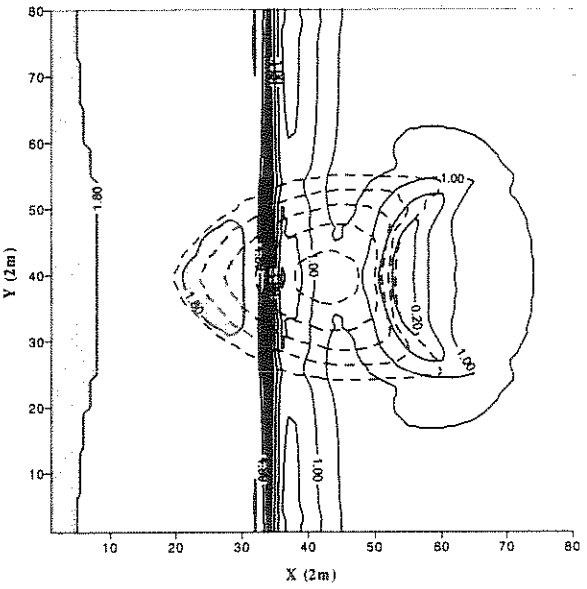

Figure 7: Horizontal distribution of wind speed of first level (about 1.5m above the ground) around and over a 5m high barchan sand dune with a 2m high windbreak hedge at 18m windward of its summit.

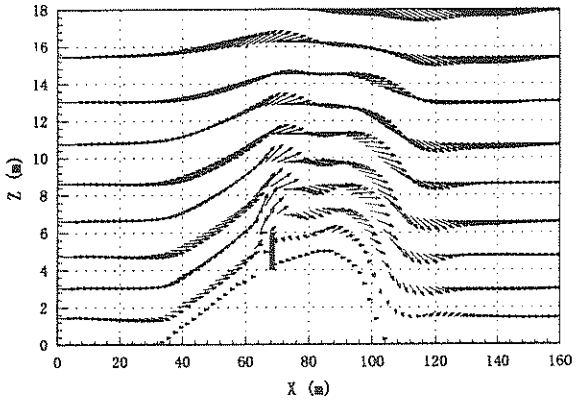

Figure 8: Vertical cross section of wind vectors over the central line of a barchan dune with a 2m high hedge installed 18m windward of the summit of the dune.

The effect of windbreak hedge on the airflow is different when the hedge installed at different places in a comlex terrain due to the intergrated effect of topography and windbreak as shown in Figure 9. Figure 9 shows horizontal distribution of wind speeds at first level (about 1.5m above the surface) over the center line of the barchan dune (Y=40) with, respectively, no windbreak, a hedge 18m windward of the dune, a hedge directly in front of the dune and a hedge 18m windward of the summit of dune. Cross section of the dune and windbreaks along the center line is also shown at the bottom of Figure 9. It is clear that strong wind was mostly reduced when hedge located 18m windward of the summit of dune. When the windbreak hedge was setup 18m windward of the dune, wind recovered when it reached the dune. When the windbreak hedge was setup in front of the dune, wind reduction was smallest due to overspeeding of sand dune. When hedge located 18m windward of the summit of dune, the

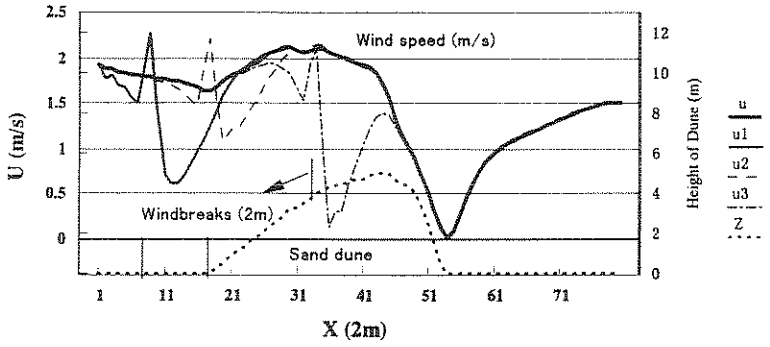

Figure 9: Horizontal distribution of wind speeds at first level (about 1.5m above the surface) over the center line of the barchan dune (Y=40) with, respectively, no windbreak (u), a hedge 18m windward of the dune (u1), a hedge directly in front of the dune (u2) and a hedge 18m windward of the summit of the dune (u3). Cross section of the dune and windbreaks along the central line is also shown at the bottom (Z).

reduction of windspeed was about two times of that when hedge located directly in front of the dune. This result shows that the best place should be at 18m-22m in front of the top of the sand dune using a 2m high windbreak hedge for preventing sand shifting around a barchan sand dune which is 5m high, 64m wide and 96m long.

4. CONCLUSONS

By introducing generalized terrain-following coordinates and Smagorinsky nonlinear eddy viscosity subgrid closure, a three-dimensional numerical model is developed. We have used the model to simulate airflow pass over windbreak hedge and a barchan sand dune and than discussed windbreak effect on airflow distribution by erecting windbreak hedges at different places. The influence of topography and windbreaks on wind distribution, for example the location of the maximum wind speed reduction and reversed flow are well simulated. Thus, our model can gives correct predictions of airflow over complex terrain with and without windbreak hedge so that the best setting place of windbreak for prevention of wind erosion may be decided by simulating the wind distribution around real terrain using the model.

Our purpose is not only simulate airflow over real complex terrain but also simulate boundary layer flow near various porosity windbreaks over complex terrain. The present model does not introduce porosity windbreak effect on airflow. In near future, we will include additional term representing the drag imposed by the porosity windbreak to the model.

5. REFERENCES

Du, M. and T. Maki, A preliminary study on the prevention of drifting sands and desertification in arid areas. *J. Agric. Meteorol.*, 48, 687-690, 1993.

Du, M. and T. Maki, Effect of Polyethylene windbreak nets on drifting sand and microclimate. *J. Agric. Meteorol.*, 52, 953-956, 1997.

Fisher, P. F. and P. Galdies, A computer model for Barchan-dune movement. *Computer & Geosci.*, 14(2), 229-253, 1988.

Heisler, G. M., and D. R. DeWalle, Effects of windbreak structure on wind flow. *Agri. Ecosyst. Environ.*, 22/23,41-69, 1988.

Judd, M. J., M. R. Raupach, and J. J. Finnigan, A wind tunnel study of turbulent flow around single and multiple wind breaks; Part 1: Velocity fields. *Boundary-Layer Meteorol.*, 80, 127-165, 1996.

Maki, T., Studies on the windbreak nets (4) Characteristics of wind speed profiles near various windbreak nets obtained by wind tunnel experiments. *J. Agric. Meteorol.*, 38, 123-133, 1982 (in Japanese with English abstract).

Maki, T., M. Du, and B. Pan, The effect of windbreaks on meteorological improvement and the prevention of wind erosion. *J. Agric. Meteorol.*, 48, 683-686, 1993.

Maki, T., B. Pan, M. Du, and R. Samejima, Effects of forest and net windbreaks on climatic improvement and protection of sand movement in arid lands of Northwestern China. *Journal of Arid Land Studies*, 5(S), 107-110, 1995.

Maki, T., M. Du, R. Samejima, and B. Pan, Movement of sand dune in Xinjiang of Northwest China and prevention of desertification by windbreak facilities in arid China. *J. Agric. Meteorol.*, 52, 633-636, 1997.

McNaughton, K. G., Effects of windbreaks on turbulent transport and microclimate. *Agri. Ecosyst. Environ.*, 22/23, 17-39, 1988.

Smagorinsky, J., General circulation experiments with the primitive equations I. the basic experiments. Mon. Weather Rev., 91, 99-164, 1963.

Van Eimern, J., R. Karschon, L. A. Razumova, and G.W. Robertson, Windbreaks and shelterbelts. *World Meteorological Organization Tech. Note* No. 59, 188 pp., 1964.

Wang, H. and E. S. Tatle, A numerical simulation of boundary-layer flow near shelterbelts. *Boundary-Layer Meteorol.*, 75, 141-173, 1995a.

Wang, H. and E. S. Tatle, Numerical simulations of shelterbelt effects on wind direction. *J. Appl. Meteor.*, 34, 2206-2219, 1995b.

Wang, H. and E. S. Tatle, On three-dimensionality of shelterbelt structure and its influences on shelter effects. *Boundary-Layer Meteorol.*, 79, 83-105, 1996.

Wilson, J. D., Numerical studies of flow through a windbreak. J. Wind Eng. Ind. *Aerodyn.*, 21, 119-154, 1985.

Wippermann, F. K. and G. Gross, The wind-induced shaping and migration of an isolated dune: a numerical experiment. *Boundary-Layer Meteorol.*, 36, 319-334, 1986.